Trends in Computational and Applied Mathematics, **25** (2024), e01766
Sociedade Brasileira de Matemática Aplicada e Computacional
Online version ISSN 2676-0029 www.scielo.br/tcam
ORIGINAL ARTICLE
doi: 10.5540/tcam.2024.025.e01766

Gaussian Pulses over Random Topographies for the Linear Euler Equations

M. V. FLAMARION[1*] and R. RIBEIRO-JR[2]

Received on June 26, 2023 / Accepted on December 19, 2023

ABSTRACT. This study investigates numerically the interaction between a Gaussian pulse and variable topography using the linear Euler equations. The impact of topography variation on the amplitude and behavior of the wave pulse is examined through numerical simulations and statistical analysis. On one hand, we show that for slowly varying topographies, the incoming pulse almost retains its shape, and little energy is transferred to the small reflected waves. On the other hand, we demonstrate that for rapidly varying topographies, the shape of the pulse is destroyed, which is different from previous studies.

Keywords: water waves, conformal mapping, Euler equations.

1 INTRODUCTION

The study of the ocean holds significant interest in its own right. The main set of equations used to model the dynamic of water waves was first derived by Isaac Newton (1687) with limited mathematical rigor. Later, Leonhard Euler (1757) derived a set of equations for the governing water wave dynamics without incorporating any dissipative effects, these set of equations become known as the Euler equations [7].

The Euler equations are used to model several problems such as ship wakes, flow of water over rocks, the formation of storms in the ocean and even atmospheric problems such as atmospheric flows encountering obstacles [2, 14]. These problems are typically approached as deterministic, where the initial state is precisely known, and the evolution of the phenomenon over time can be computed using the Euler equations. However, in many cases, the scarcity of data for initializing deterministic models presents a challenge. In such instances, assuming random initial states becomes preferable, allowing for the study and formulation of statistically reliable predictions [8, 9, 21, 22, 25]. Analogously, the medium in which a wave propagates can also be considered random [1, 12, 13, 20]. In particular, we mention the work of Nachbin and Solna [20] which

*Corresponding author: Marcelo V. Flamarion – E-mail: flamarion@ita.br
[1]Aeronautics Institute of Technology (ITA), Department of Mathematics, 12228-900, São José dos Campos, São Paulo, Brazil Email: flamarion@ita.br https://orcid.org/0000-0001-5637-7454
[2]Federal University of Paraná (UFPR), Departamento de Matemática, Centro Politécnico, Jardim das Américas, Caixa Postal 19081, Curitiba, PR, 81531-980, Brazil – E-mail: robertoribeiro@ufpr.br https://orcid.org/0000-0001-5077-3026

investigates the effect of a random topography on the Gaussian pulse on the free surface. Among their results, they showed that the pulse experience an apparent diffusion, which is featured by a loss in amplitude of the incoming pulse after passing over a rapidly varying topography.

The Euler equations have been widely utilized in various studies. For example, Choi and Camassa [5] numerically computed solitary waves over a flat bottom , while Choi [4] investigated these waves in the presence of a vertically sheared current with constant vorticity. Ribeiro-Jr et al. [23] analyzed particle trajectories and pressure within the fluid bulk. Nachbin [16] introduced a conformal mapping technique to flatten uneven topography and derived an asymptotic Boussinesq-type equation with variable coefficients. Flamarion et al. [10] examined particle trajectories for the linear Euler equations considering a linear sheared current and variable topography. Moreover, the Euler equations have found applications in the study of free boundary problems at small scales, such as the motion of a fluid droplet (silicon) walking on the surface of a vibrating bath. This phenomenon exhibits similarities to the wave-particle duality observed in quantum mechanics [3, 6, 15]. Nachbin and colleagues extensively explored the role of free surface waves as a spontaneous mechanism for synchronizing oscillating droplets confined within various types of cavities, through the Schwarz-Christoffel mapping [17, 18, 19].

The objective of this study is to investigate the behaviour of the interaction between a Gaussian pulse with a random topography. As our model is deterministic, we conduct numerous Monte Carlo simulations with randomly generated topographies sharing identical statistical characteristics. The primary aim of this study is to investigate statistically the effective behavior resulting from the interaction between an initial Gaussian pulse and randomly smooth topographies, an approach not fully explored in the literature.

Our study indicates that when the topography exhibits slow variation (small wavenumbers), the resulting wave shape undergoes minimal changes, with the amplitude remaining nearly constant. As the wavenumber increases, fluctuations in the resulting wave amplitude emerge, yet its shape still resembles the initial Gaussian bell, albeit with additional tails caused by the pulse-topography interaction. Ultimately, as the wavenumber further increases, the resulting wave experiences a change in shape, tending to split into two pulses. This division results in a substantial difference in amplitude between the leading wave and the initial pulse.

This article is organized as follows: In Section 2, we present the mathematical formulation of the Euler equations. In Section 3, we describe the conformal mapping technique and rewrite the Euler equations in the canonical domain, which is a uniform strip. The numerical methods are presented in Section 4. In Section 5, we present the main results, and the final considerations are discussed in Section 6.

2 MATHEMATICAL FORMULATION

We examine the behavior of a two-dimensional, irrotational flow in a finite depth channel filled with an inviscid and incompressible fluid of constant density. The channel includes a variable topography and features a free surface wave ($\zeta(x,t)$) affected by gravity. The governing equations,

known as the Euler equations and referenced in [26], describe the dynamics of the free surface and the potential velocity ($\tilde{\phi}(x,y,t)$). These equations can be expressed in dimensionless form as

$$\begin{aligned}
&\mu^2\tilde{\phi}_{xx}+\tilde{\phi}_{yy}=0 \text{ for } h(x)<y<\varepsilon\zeta(x,t),\\
&\tilde{\phi}_y=\mu^2\tilde{\phi}_x h_x \text{ at } y=h(x),\\
&\zeta_t+\varepsilon\tilde{\phi}_x\zeta_x-\frac{1}{\mu^2}\tilde{\phi}_y=0 \text{ at } y=\varepsilon\zeta(x,t),\\
&\tilde{\phi}_t+\frac{\varepsilon}{2}\left(\tilde{\phi}_x^2+\frac{1}{\mu^2}\tilde{\phi}_y^2\right)+\zeta=0 \text{ at } y=\varepsilon\zeta(x,t),
\end{aligned}$$

where ε is the nonlinearity parameter, which measures the ratio between a typical wave amplitude and the depth channel, and μ is the shallow-water/long-wave parameter which measures the ratio between the depth channel and a characteristic wavelenght. For computational purposes, it is convenient to consider the new scaling $y\to\mu y$. In this new scaling, the potential velocity is a harmonic function, thus the Euler equations become

$$\begin{aligned}
&\tilde{\phi}_{xx}+\tilde{\phi}_{yy}=0 \text{ for } \mu h(x)<y<\varepsilon\mu\zeta(x,t),\\
&\tilde{\phi}_y=\mu\tilde{\phi}_x h_x \text{ at } y=\mu h(x),\\
&\zeta_t+\varepsilon\tilde{\phi}_x\zeta_x-\frac{1}{\mu}\tilde{\phi}_y=0 \text{ at } y=\varepsilon\mu\zeta(x,t),\\
&\tilde{\phi}_t+\frac{\varepsilon}{2}\left(\tilde{\phi}_x^2+\frac{1}{\mu}\tilde{\phi}_y^2\right)+\zeta=0 \text{ at } y=\varepsilon\mu\zeta(x,t),
\end{aligned}\tag{2.1}$$

We are interested in investigating solutions of (2.1) in the linear regime ($\varepsilon=0$) and weakly dispersive regime ($\mu\approx 0$). Under these assumptions we have the linear system of equations

$$\begin{aligned}
&\tilde{\phi}_{xx}+\tilde{\phi}_{yy}=0 \text{ for } \mu h(x)<y<0,\\
&\tilde{\phi}_y=\mu\tilde{\phi}_x h_x \text{ at } y=\mu h(x),\\
&\zeta_t-\frac{1}{\mu}\tilde{\phi}_y=0 \text{ at } y=0,\\
&\tilde{\phi}_t+\zeta=0 \text{ at } y=0.
\end{aligned}\tag{2.2}$$

When the bottom is flat, the phase speed of the linear waves are given by [26]

$$c(k)=\sqrt{\frac{\tanh(\mu k)}{\mu k}}.\tag{2.3}$$

We recall that this is for example the speed of the crest of the wave as it propagates. Notice that in the limit $\mu\to 0$, all linear waves travel with the same speed $c=1$.

3 CONFORMAL MAPPING AND NUMERICAL METHODS

We remember that one of the primary characteristics of conformal mappings is the conformal invariance of the Laplacian operator. Consequently, to solve equation (2.2), we can employ a

conformal mapping and address it within a simpler domain. For this purpose, we construct a conformal mapping denoted as

$$z(\xi,\eta) = x(\xi,\eta) + iy(\xi,\eta),$$

which flattens the bottom topography and maps a strip of width D onto the fluid domain, where the value of D is determined afterwards. This conformal mapping satisfies the boundary conditions

$$y(\xi,0) = 0 \quad \text{and} \quad y(\xi,-D) = \mu \mathbf{H}(\xi), \tag{3.1}$$

where $\mathbf{H}(\xi) = h(x(\xi,-D))$. The formulation presented here is identical to the one described in [11], hence we will briefly summarize the main steps.

Let $\phi(\xi,\eta,t) = \bar{\phi}(x(\xi,\eta),y(\xi,\eta),t)$ represent the potential velocity in the canonical domain. By utilizing the Dirichlet-to-Neumann condition, we obtain

$$\phi_\eta(\xi,0,t) = \mathscr{F}^{-1}\left[k_j \tanh(k_j\mu)\widehat{\phi}(k_j,0,t)\right]. \tag{3.2}$$

Furthermore, at $\eta = 0$, we have

$$\begin{aligned} &\phi_t + \zeta = 0, \\ &\zeta_t - \frac{1}{\mu M(\xi)}\phi_\eta = 0, \end{aligned} \tag{3.3}$$

where in the shallow-water regime ($\mu \approx 0$), we have the limit

$$M(\xi) = x_\xi(\xi,0) = -\mathbf{H}(\xi).$$

Therefore, all the topography information is carried in the metric coefficient $M(\xi)$.

4 NUMERICAL METHODS

We solve (3.2) and (3.3) in a computational domain $[-L,L]$, with a uniform grid with N_ξ points and step $\Delta\xi = 2L/N_\xi$. The spatial derivatives are computed using the Fast Fourier Transform (FFT) [24]. In addition, the time advance of the system (3.3) is computed through the Runge-Kutta fourth order method (RK4) with time step Δt. The numerical method proposed here is implemented in MATLAB and it consists of a variation of the code available in [11].

The initial wave profile is taken as

$$\zeta(\xi,0) = \exp\Big(-(\xi-\xi_0)^2\Big),$$

where ξ_0 is its initial location. The initial potential velocity is taken as

$$\phi_\xi(\xi,0,0) = \mathscr{F}^{-1}\Big[\frac{-ik}{c(k)}\widehat{\zeta}(k,0)\Big],$$

where $c(k)$ is given by (2.3) and $\mathscr{F}^{-1}$ denotes the inverse Fourier transform. This choice of initial data guarantees that the solution travels to right when the bottom is flat. A zero-mean random topography is modeled as the Fourier series and contains N harmonics

$$M(\xi) = 1 + \left[\sum_{i=1}^{N} \sqrt{2S(k_i)\Delta k} \cos(k_i \xi + \varphi_i) \right] \chi_{[-L_0, L_0]}(\xi), \tag{4.1}$$

where $\chi_{[-L_0,L_0]}(\xi)$ is the characteristic function in the interval $[-L_0, L_0]$, $S(k)$ is an initial power spectrum, $k_i = i\Delta k$ and Δk is a sampling wave number, and a phase φ_i is a random variable, uniformly distributed in the interval $(0, 2\pi)$. The length of initial realization is $L = 2\pi/\Delta k$. An initial power spectrum is assumed to have a Gaussian distribuition

$$S(k) = \frac{Q_0}{\sigma\sqrt{2\pi}} \exp\Big(-\frac{1}{2} \frac{(k-k_0)^2}{\sigma^2} \Big). \tag{4.2}$$

In what follows we set the following parameters: $\Delta k = 0.013$, $L = 2\pi/\Delta k$, $N = 256$, $N_\xi = 2^{12}$, $\Delta t = 0.005$, $\sigma = 0.27$, $Q_0 = 0.01$, $\xi_0 = -60$ and $L_0 = 50$, $\mu = 0.001$.

5 RESULTS

We examine various values for the peak wavenumber, denoted as k_0 , which play a crucial role in determining the rate of topography variation. When $k_0 \gg 1$, the topography is said to be rapidly varying, while for $k_0 \ll 1$, the topography is said to be slowly varying. Consequently, we focus our simulations on investigating three distinct regimes of k_0, namely, intermediate varying, rapidly and slowly.

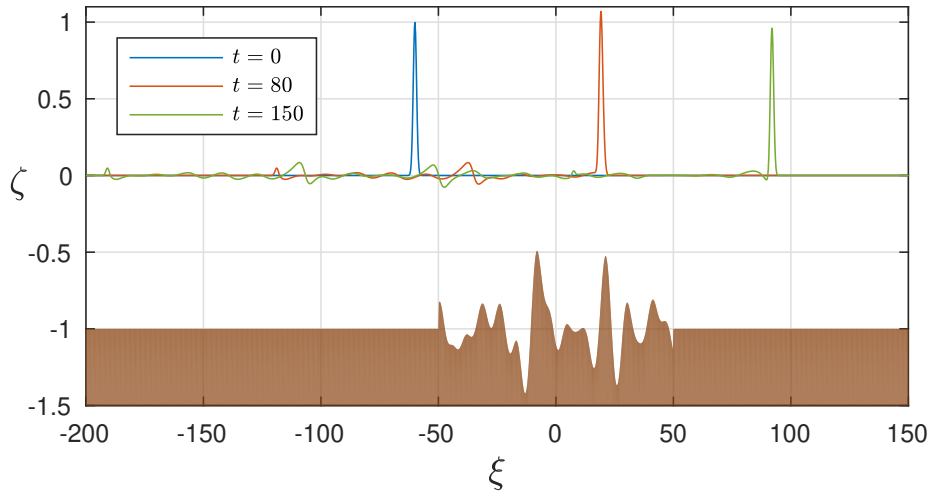

Figure 1: The Gaussian pulse evolution at different times for the wavenumber peak $k_0 = 0.5$.

We begin by considering the case where $k_0 = 0.5$. In this scenario, the Gaussian-shaped wave pulse propagates without significant reflections or dispersion effects in the positive direction.

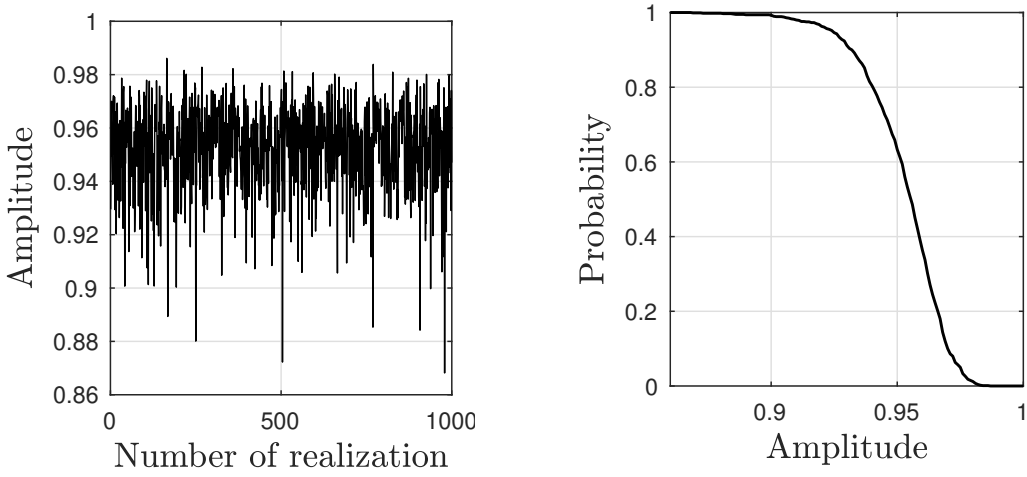

Figure 2: Left: The maximum amplitude of the pulse after passing over the topography (time $t = 150$). Right: The distribution of the amplitudes over 1000 realizations for the Gaussian pulse at $t = 150$. Parameters: $k_0 = 0.5$.

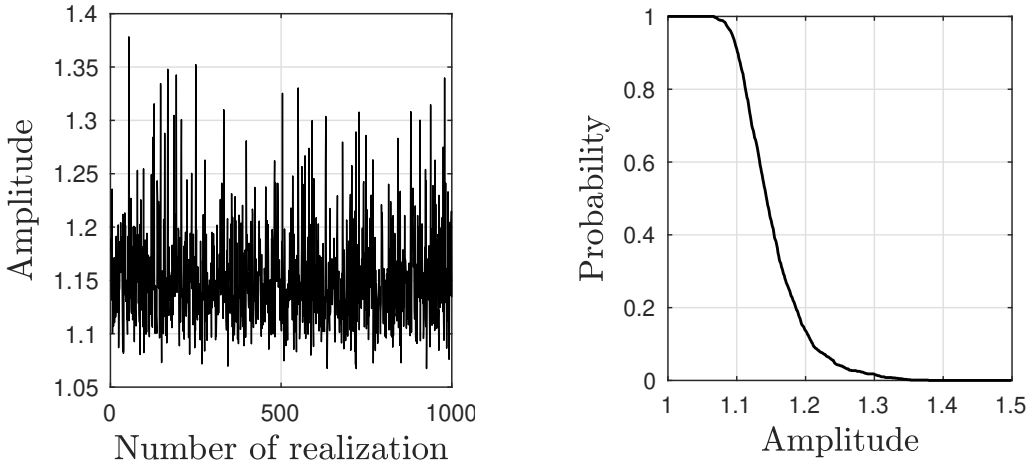

Figure 3: Left: The maximum amplitude of the pulse over time. Right: The distribution of the amplitudes over 1000 realizations for the Gaussian pulse over time. Parameters: $k_0 = 0.5$.

However, when the wave encounters the intermediate varying topography, its amplitude undergoes variations, leading to the generation of reflected waves. This phenomenon is illustrated in detail in Figure 1, which demonstrates the interaction between the wave pulse and the topography. The interaction with the variable topography causes the bell-shaped pulse to lose energy, resulting in a decrease in its amplitude. This energy is then transferred to the reflected waves propagating in the opposite direction. To gain a deeper understanding of this behavior, we conducted numerous Monte Carlo simulations to draw statistical conclusions regarding the pulse-

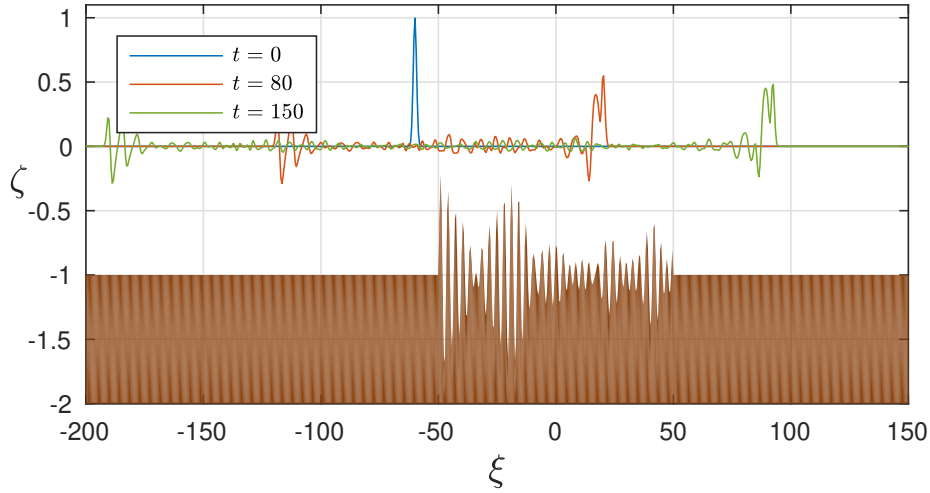

Figure 4: The Gaussian pulse evolution at different times for the wavenumber peak $k_0 = 2$.

topography interaction. Figures 2 and 3 provide detailed information on the maximum amplitude variation of the pulse after interacting with the topography and throughout the entire simulation, respectively. These figures highlight the statistical nature of the amplitude fluctuations, with the standard deviation of the amplitude on the order of $\mathcal{O}(0.1)$ following the interaction. The influence of the topography on the amplitude-wave behavior becomes evident. To further explore the statistical aspects of the pulse-topography interaction, we examine the probability distribution of the output wave amplitude during the interaction. Figures 2 (right) and 3 (right) display the probability distribution of the output wave maximum amplitude and the maximum amplitude during the interaction, respectively. These probability distributions provide valuable insights into the behavior of the pulse as it interacts with the variable topography. For instance, in Figure 2 (left) we see that the probability of obtaining an output wave with amplitude greater than 0.95 is approximately 60%.

Next, we investigate the case where $k_0 = 2$. In this regime, the resulting pulse shape undergoes a significant transformation upon interacting with the topography, as depicted in Figure 4. The interaction between the Gaussian pulse and the topography becomes more pronounced, resulting in wave reflection. In order to give more details, we monitor the changes in the maximum amplitude of the output wave and the wave during propagation, as shown in Figures 5 and 6, respectively. It is important to note that compared to the previous case, the fluctuation of the output wave amplitude is more prominent. This increase in fluctuation is a direct consequence of the stronger interaction between the pulse and the topography. The reflection of waves caused by this interaction introduces additional complexity to the system, resulting in larger amplitude variations in the output wave. Notice that differently from the previous case we see that the probability of obtaining an output wave with amplitude greater than 0.90 is zero, see Figure 5 (left).

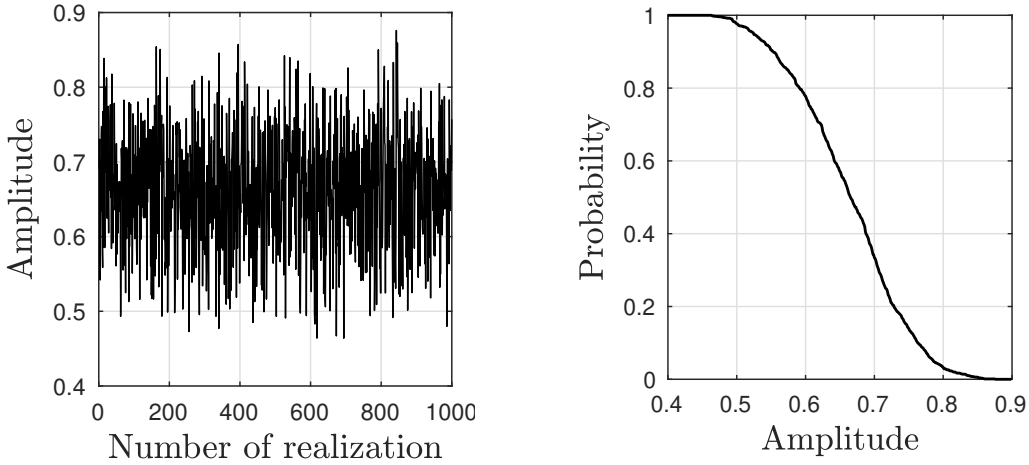

Figure 5: Left: The maximum amplitude of the pulse after passing over the topography (time $t = 150$). Right: The distribution of the amplitudes over 1000 realizations for the Gaussian pulse at $t = 150$. Parameters: $k_0 = 2$.

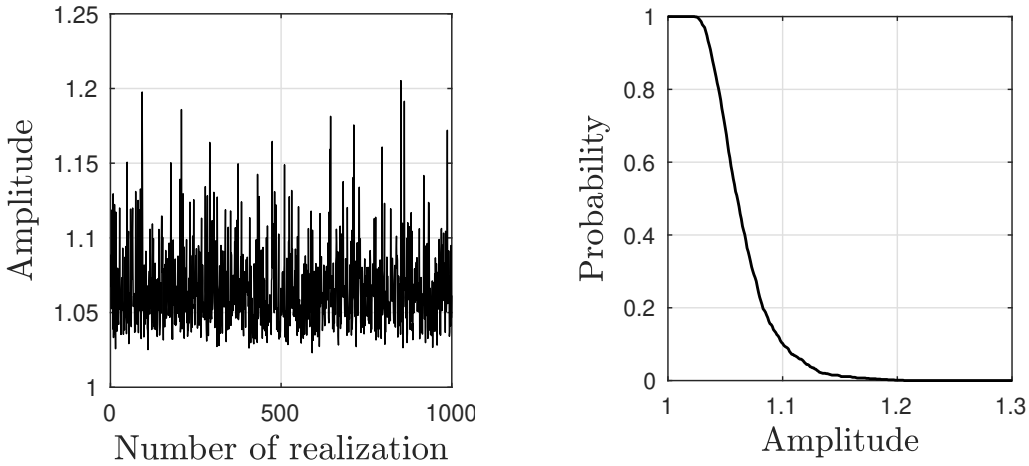

Figure 6: Left: The maximum amplitude of the pulse over time. Right: The distribution of the amplitudes over 1000 realizations for the Gaussian pulse over time. Parameters: $k_0 = 2$.

Lastly, we consider the case where the topography varies slowly (k_0 is small). We set $k_0 = 0.05$. Figure 7 displays a typical wave solution at different times for slowly varying topography. Observe that its amplitude remains almost unchanged after the Gaussian pulse interacts with the topography. Additionally, we note that the reflected waves have less energy compared to the previous cases. This behavior is also evident from the statistical perspective, as shown in Figure 8 for the output wave. The fluctuation in the wave amplitude is very small, indicating that its initial shape is almost preserved. The same holds true for the fluctuation of the Gaussian pulse as it

passes over the topography, as seen in Figure 9. It is worth to mention that the probability of the output pulse retains 99% of its initial amplitude is about 80%.

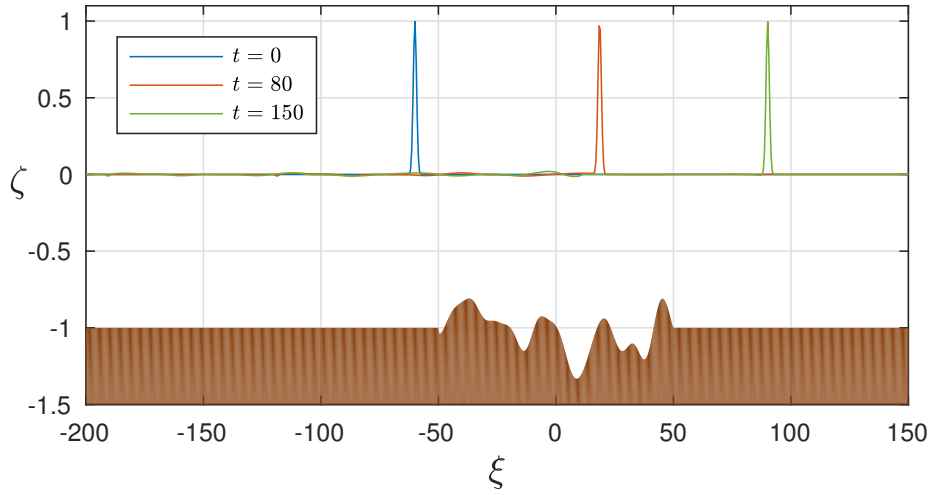

Figure 7: The Gaussian pulse evolution at different times for the wavenumber peak $k_0 = 0.05$.

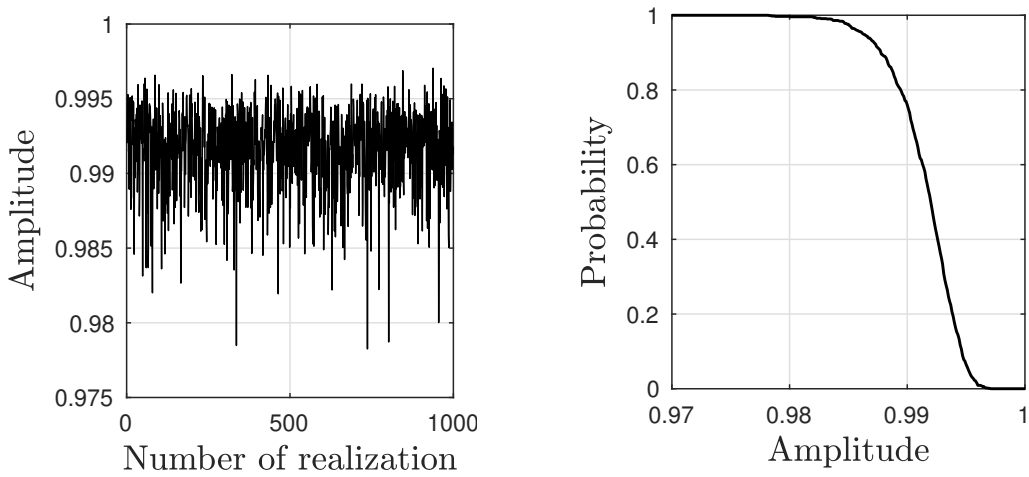

Figure 8: Left: The maximum amplitudes of the pulse after passing over the topography (time $t = 150$). Right: The distribution of the amplitudes over 1000 realizations for the Gaussian pulse at $t = 150$. Parameters: $k_0 = 0.05$.

In summary, our investigation demonstrates that different values of the peak wavenumber k_0, which results in different topographies, significantly affecting the amplitude and behavior of the wave pulse. These results ties with the study of Nachbin and Solna [20]. We notice that the changing in the dynamic presented in this work is different from the ones reported by Flamarion

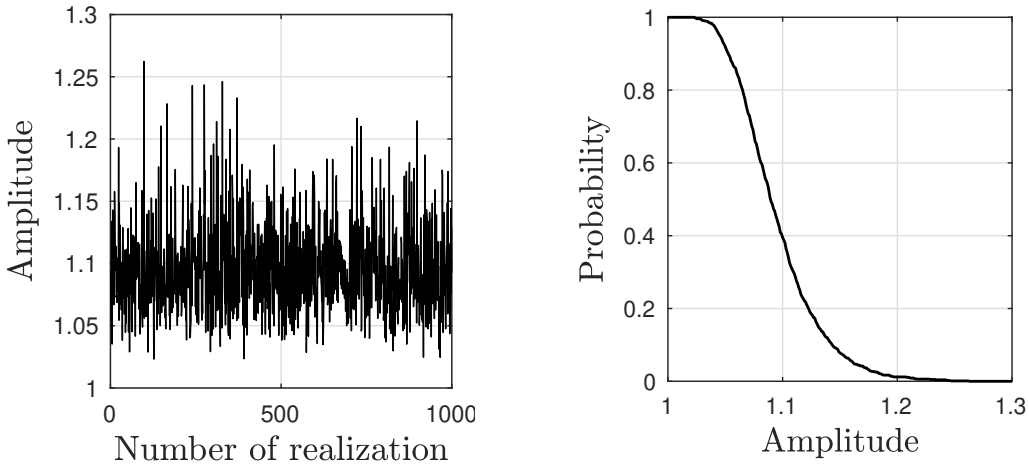

Figure 9: Left: The maximum amplitude of the pulse over time. Right: The distribution of the amplitudes over 1000 realizations for the Gaussian pulse over time. Parameters: $k_0 = 0.05$.

and Ribeiro-Jr [11]. In this article, the authors showed that a monochromatic rapidly varying topography barely affects the shape of the pulse, while a slowly varying topography causes a considerable variation in amplitude and an increasing of reflected waves. This occurs because only monochromatic topographies are considered in [11]. Therefore, our study shows that when the topography is modeled by a series of Fourier modes the wave field changes considerably. The statistical analysis of the pulse-topography interaction sheds light on the energy transfer and amplitude fluctuations involved in the process.

6 CONCLUSIONS

In conclusion, our investigation into the interaction between wave pulses and variable topography has provided valuable insights into the behavior of the system. On one hand, we show that for slowly varying topographies, the incoming pulse almost retains its shape, and little energy is transferred to the small reflected waves. On the other hand, we demonstrate that for rapidly varying topographies, the shape of the pulse is destroyed. This article contributes to a deeper understanding of wave propagation in variable topographic environments. Further studies can be built upon this work to explore additional aspects of wave-topography interactions for more complex models.

Acknowledgments

The authors are grateful to the unknown referees for their constructive comments and suggestions which improved the manuscript. The work of M.V.F. and R.R.Jr was supported in part by National Council Scientific and Technological Development (CNPq) under Chamada CNPq/MCTI/N^o 10/2023-Universal.

REFERENCES

[1] D.G. Alfaro-Vigo, J. Fouque, J. Garnier & A. Nachbin. Robustness of time reversal for waves in time-dependent random media. *Stochastic Process and Applications*, **113** (2004), 289–313.

[2] P. Baines. "Topographic effects in stratified flows". Cambridge University Press (1995).

[3] J. Bush, Y. Couder, T. Gilet, P.A. Milewski & A. Nachbin. Introduction to focus issue on hydrodynamic quantum analogs. *Chaos*, **28** (2018), 096110.

[4] W. Choi. Nonlinear surface waves interacting with a linear shear current. *Math Comput Simul*, **80** (2009), 29–36.

[5] W. Choi & R. Camassa. Exact evolution equations for surface waves. *J Eng Mech*, **25** (1999), 756–760.

[6] Y. Couder & E.T. Fort. Single-particle diffraction and interference at a macroscopic scale. *Phys Rev Lett*, **97** (2006), 154101.

[7] A.D.D. Craik. The Origins of Water Wave Theory. *Annu Rev Fluid Mech*, **39** (2004), 1.

[8] E.G. Didenkulova, A.V. Slunyaev & E.N. Pelinovsky. Numerical simulation of random bimodal wave systems in the KdV framework. *Eur. J. Mech. B Fluids*, **78** (2019), 21–31.

[9] D. Dutykh. Evolution of random wave fields in the water of finite depth. *Procedia IUTAM*, **11** (2014), 34–43.

[10] M.V. Flamarion, A. Nachbin & R. Ribeiro-Jr. Time-dependent Kelvin cat-eye structure due to current-topography interaction. *J Fluid Mech*, **889** (2020), A11.

[11] M.V. Flamarion & R. Ribeiro-Jr. A numerical study of linear long water waves over variable topographies using a conformal mapping. *Trends in Computational and Applied Mathematics*, **23**(4) (2022), 625–638.

[12] J. Fouque, J. Garnier & A. Nachbin. Time reversal for dispersive waves in random media. *SIAM J. Appl. Math.*, **64**(5) (2004), 1819–1836.

[13] J. Fouque, J. Garnier, A. Nachbin & K. Solna. Time reversal refocusing for point source in randomly layered media. *Wave Motion*, **42**(3) (2004), 238–260.

[14] R.S. Johnson. Models for the formation of a critical layer in water wave propagation. *Phil Trans R Soc A*, **370** (2012), 1638–1660.

[15] P.A. Milewski, C.A. Galeano-Rios, A. Nachbin & J. Bush. Faraday Pilot-wave dynamics: modelling and computation. *J Fluid Mech*, **778** (2015), 361–388.

[16] A. Nachbin. A terrain-following Boussinesq system. *SIAM J Appl Maths*, **63**(4) (2004), 905–922.

[17] A. Nachbin. Walking droplets correlated at a distance. *Chaos*, **28** (2018), 096110.

[18] A. Nachbin. Kuramoto-Like Synchronization Mediated through Faraday Surface Waves. *Fluids*, **5**(4) (2020), 226.

[19] A. Nachbin, P.A. Milewski & J. Bush. Tunneling with a hydrodynamic pilot-wave model. *Phys Rev Fluids*, **2**(034801) (2017), 096110.

[20] A. Nachbin & K. Solna. Apparent diffusion due to topographic microstructure in shallow waters. *Phys Fluids*, **2**(034801) (2003).

[21] E. Pelinovsky & A. Sergeeva. Numerical modeling of the KdV random wave field. *Eur. J. Mech. B Fluids*, **15**(1) (2006), 66–77.

[22] E. Pelinovsky & E. Shurgalina. Nonlinear dynamics of a soliton gas: Modified Korteweg-de Vries equation framework. *Phys. Lett. A.*, **380** (2016), 2049–2053.

[23] R. Ribeiro-Jr, P.A. Milewski & A. Nachbin. Flow structure beneath rotational water waves with stagnation points. *J Fluid Mech*, **812** (2017), 792–814.

[24] L.N. Trefethen. "Spectral Methods in MATLAB". Philadelphia: SIAM (2001).

[25] C. Viotti, D. Dutykh, J.M. Dudley & F. Dias. Emergence of coherent wave groups in deep-water random sea. *Phys Rev E.*, **87**(063001) (2013).

[26] G.B. Whitham. "Linear and nonlinear water waves". John Wiley & Sons, Inc (1974).

How to cite

M.V. Flamarion & R. Ribeiro-Jr. Gaussian pulses over random topographies for the linear Euler equations. *Trends in Computational and Applied Mathematics*, **25**(2024), e01766. doi: 10.5540/tcam.2024.025.e01766.